Control of residual oxygen of the process atmosphere during laser-powder bed fusion processing of Ti-6Al-4V

Downloaded from: https://research.chalmers.se, 2021-08-31 11:53 UTC

Citation for the original published paper (version of record):

Pauzon, C., Dietrich, K., Forêt, P. et al (2021)
Control of residual oxygen of the process atmosphere during laser-powder bed fusion processing of Ti-6Al-4V
Additive Manufacturing, 38
http://dx.doi.org/10.1016/j.addma.2020.101765

N.B. When citing this work, cite the original published paper.

research.chalmers.se offers the possibility of retrieving research publications produced at Chalmers University of Technology.
It covers all kind of research output: articles, dissertations, conference papers, reports etc. since 2004.
research.chalmers.se is administrated and maintained by Chalmers Library

(article starts on next page)

Additive Manufacturing 38 (2021) 101765

Contents lists available at ScienceDirect

Additive Manufacturing

journal homepage: www.elsevier.com/locate/addma

Research Paper

Control of residual oxygen of the process atmosphere during laser-powder bed fusion processing of Ti-6Al-4V

C. Pauzon [a,*], K. Dietrich [b], P. Forêt [c], S. Dubiez-Le Goff [c], E. Hryha [a], G. Witt [b]

[a] Department of Industrial and Materials Science, Chalmers University of Technology, SE-41296 Göteborg, Sweden
[b] University of Duisburg-Essen, Lotharstrasse 1, DE-47057 Duisburg, Germany
[c] Linde AG, Carl-von-Linde-Strasse 25, DE-85716 Unterschleissheim, Germany

ARTICLE INFO

Keywords:
L-PBF
Ti-6Al-4V
Process atmosphere
Residual oxygen
XRD
XPS

ABSTRACT

The effect of the residual oxygen concentration in the process atmosphere during laser-powder bed fusion (L-PBF) of Ti-6Al-4V was investigated, using an external oxygen monitoring system equipped with two types of oxygen sensors typically used in L-PBF hardware: a lambda probe and an electrochemical oxygen sensor. The recordings of the oxygen variations during L-PBF highlighted that the electrochemical sensor is more reliable than the lambda probe, whose signal showed a maximum deviation of about 700 ppm O_2 after 7 h, attributed to its sensitivity to hydrogen present in the system. The study revealed that proper monitoring of the oxygen in the laboratory scale L-PBF system used is necessary to limit oxygen and nitrogen pick-ups by the built material. Concentrations as high as 2200 ppm O_2 and 500 ppm N_2 in the Ti-6Al-4V part built under standard conditions were measured, compared to maximum levels of 1800 ppm O_2 and 250 ppm N_2 with the external oxygen control. In addition, the findings underline the critical effect of the component design, such as the high aspect ratio columns or the lattice structures, on the heat accumulation in case of Ti-6Al-4V, leading to enhanced oxygen and nitrogen pick-up, as high as 600 ppm O_2 and 150 ppm N_2 difference between the bottom and top of the cylindrical samples of 70 mm height used in this study. The determination of tensile properties of samples built at different heights put in evidence the detrimental effect of the oxygen increase with build height on the ductility, which decreased from 12% to below 6% between the bottom and top positions. This work highlights that the possible presence of impurities in the L-PBF atmosphere can have harmful impact on the properties of Ti-6Al-4V components, which can be mitigated adjusting the oxygen control system.

1. Introduction

The study of the process gas as a parameter of its own in the case of the laser-powder bed fusion (L-PBF) process has become a necessary step towards gaining a better understanding of the laser-powder-atmosphere interactions [1–4]. Since the early development of industrial L-PBF systems, the role of the gas was primarily limited to establishing a laminar flow allowing for the removal of projections from the laser path [5,6] and ensuring a relatively low oxygen level, not necessarily low enough to inhibit oxidation reactions promoted by the high heat inputs. Even though more sophisticated techniques have been developed to establish the process atmosphere [7], doing so is still mostly achieved by purging the closed process volume with inert gas, such as argon, until the oxygen level is significantly lowered. Other impurities, such as water vapour and nitrogen, are removed in the same manner, but their content is not directly measured and instead is related to the residual oxygen content. While most systems typically set this value to 1000 ppm of oxygen, some machines offer more freedom for the operator to select this setpoint. As this setpoint is reached upon purging, the inert gas is reused by a recirculation system via a pump.

The importance of reaching and establishing this setpoint should be determined based on the sensitivity of the material processed, in which some materials exhibit higher sensitivity to residual oxygen, such as Ti- and Al- alloys [8], while others are more robust, such as 316 L stainless steel [9]. From the L-PBF processing point of view, this setpoint also depends on several aspects, including the machine tightness, its oxygen control system, the purity of the inert gas employed, the oxygen and water vapour contents present in the feedstock material, the humidity in the laboratory air, and so on. While for example, powder chemistry and laboratory air quality can be measured and monitored by the operator,

* Corresponding author.
E-mail address: pauzon@chalmers.se (C. Pauzon).

https://doi.org/10.1016/j.addma.2020.101765
Received 23 September 2020; Received in revised form 14 November 2020; Accepted 5 December 2020
Available online 13 December 2020
2214-8604/© 2020 The Author(s). Published by Elsevier B.V. This is an open access article under the CC BY license (http://creativecommons.org/licenses/by/4.0/).

limited actions can be taken to cope with machine-related closed settings.

Ti-6Al-4V is an alloy that has been processed by L-PBF since the early adoption of this technology, as it finds direct applications in various sectors, such as medical [10]. Due to the high affinity of Ti and Al for oxygen [11], it is sensitive to oxygen dissolution and embrittlement. The solubility of oxygen in α-Ti is important (33 at%) [12]. In addition to the stabilization of the α phase, oxygen can be responsible for solution strengthening of Ti-6Al-4V. The oxygen in solution typically introduces resistance to the dislocation motion, which is attributed to the interaction between the dislocations and the lattice strains around the solute atom [13,14]. This can be observed as an increase of 100 MPa in strength for each addition of 0.01 wt% of oxygen [15], which also critically affects the ductility. Therefore, critical applications such as aerospace have tougher requirements on oxygen contents. Furthermore, nitrogen has an important solubility in α-Ti and can strengthen it by solid solution or form nitrides such as TiN and Ti_2N. This is sometimes intentionally introduced by nitridation to enhance the wear resistance of steels or titanium alloys.

Some recent studies have highlighted that enhanced oxygen pick-up during L-PBF of Ti-6Al-4V, depending on the part design and laser scanning strategies involved, significantly affects its ductility. Barba et al. [15] demonstrated that thin Ti-6Al-4V samples are rich in oxygen, which was attributed to their high surface-to-volume ratio and enhanced diffusion of the residual oxygen present during the process and eventually during the post-heat treatments. Velasco-Castro et al. [16] artificially raised the oxygen levels of Ti-6Al-4V lattice structures by implementing a re-melting strategy. This also had a detrimental effect on the ductility of the struts, which experienced a ductile-to-brittle transition with increasing laser passes, and the overall strength measured in compression decayed. In addition, Dietrich et al. [8] demonstrated that the fatigue life of horizontal Ti-6Al-4V samples decreased with the oxygen level increasing in the L-PBF process atmosphere.

The principal aim of this study was to understand the influence of the oxygen level in the processing atmosphere, measured using specially developed control system, on the processing and properties of an alloy known to be sensitive to oxygen pick-up: Ti-6Al-4V. A small-size industrial L-PBF machine was used to produce simple columns under normal condition, using machine monitoring system to control the oxygen level, and under the control of an external oxygen monitoring system. The goal was to highlight the possible effect of the exposition to impurities, such as oxygen and nitrogen, during L-PBF on the bulk and surface properties of the produced Ti-6Al-4V.

2. Materials and methods

Gas atomized Ti-6Al-4V Grade 23 powder from Heraeus (see chemical composition in Table 1) was used to produce parts by L-PBF using a TruPrint1000 machine from Trumpf GmbH, which is a laboratory scale system. The powder particle size distribution was measured using a CAMSIZER X2, and D10, D50, and D90 were 16, 25, 44 μm, respectively. Standard laser parameters using a 20 μm layer thickness developed by Trumpf GmbH for this machine model were employed to build the components studied in this work (under the license *TruPrint_1000_-Spot30_Ti64_ELI-A_Surface_v2.0*), without baseplate pre-heating (not possible for the hardware utilized). The TruPrint1000 uses a lambda probe to monitor the oxygen concentration in the process atmosphere. The sensor is placed at the end of the recirculation system just before the gas enters the building chamber again.

Table 1
Chemical composition of the used Ti-6Al-4V powder. The Al and V contents were specified by the powder supplier, and the N and O contents were measured by combustion gas analysis using a LECO ONH836.

Al [wt%]	V [wt%]	O [ppm]	N [ppm]
6.21	3.97	1051	150

High-quality technical argon was fed into the machine to generate a protective atmosphere: Argon 5.0, which contains less than 10 ppm impurities, such as H_2O, O_2, C_nH_m, or N_2. The L-PBF machine generates the process conditions by flushing the build volume with the inert gas and therefore diluting the air present initially. During the build job, the inert atmosphere is recirculated to establish a laminar flow over the baseplate on which the components are printed. The oxygen concentration is measured at the top of the build chamber and within the recirculation system. An additional inert gas flow is used to counteract possible increases in oxygen if the level exceeds that specified by the operator of the machine.

In the current study, an external monitoring system, the ADDvanceO2® precision (Linde GmbH), is employed to accurately measure possible variations in the residual oxygen level in the process atmosphere and take corrective actions, if necessary. This system has been introduced and described in previous works in detail [8,9,17,18]. It can be connected to different models of L-PBF machines and offers high-precision monitoring of the process atmosphere. Moreover, it is equipped with different sensors, among which are an electrochemical oxygen sensor, a lambda probe, and a dew point sensor. In this work, it was employed to measure the variation in residual oxygen during a standard printing build job. Therefore, the L-PBF machine was controlling the oxygen level during processing, and the external system was used only to measure the actual oxygen level close to the powder bed. This was then compared with a build job for which the external system was actively used to ensure a stable oxygen level. For both build jobs, the targeted oxygen content was set to 100 ppm O_2. Therefore, this value was set on the L-PBF machine and later on the external monitoring system, as well.

The build job conducted under these two conditions consisted of a round column 22 mm in diameter and 70 mm in height, placed at the centre of the round baseplate that is 100 mm in diameter for the TruPrint1000. The two produced columns were characterized thoroughly based on their surface and bulk properties. The oxygen and nitrogen contents of the bulk along the column's height were measured via combustion gas analysis using a LECO ONH836. To evaluate the chemical composition of the bulk material, the built columns were machined to a smaller diameter of 5 mm. These were further cracked into smaller pieces using pliers. The variation of Vickers hardness (HV10) along the height was measured using a DuraScan20 from EmcoTest on the polished cross-section of the columns. The values reported are averages taken on at least three measurements at a given position along the building direction. Sections of the columns located at their bottom (close to the baseplate), middle (half-height), and top (last layers) were cut using a diamond saw and extracted. These were embedded in conductive resin, ground, and finally polished with OP-S admixed with 30% hydrogen peroxide. Porosity was measured on these polished surfaces by light optical microscopy (LOM) using a Keyence Series 6000. The polished cross-sections were etched using a Kroll solution (92 mL water, 6 mL nitric acid, 2 mL hydrofluoric acid) to reveal the microstructures along the building direction, which were documented by high-resolution scanning electron microscopy (HR SEM) using a LEO Gemini 1550. Moreover, HR SEM was conducted on the surfaces for the three different positions analysed in detail. X-ray diffraction (XRD) was conducted on the column's bulk for phase analysis with a PANalytical X'Pert Pro diffractometer with a Cu Kα radiation operated at 45 kV and 40 mA in the 30–90° range. XRD was also performed on the surface for qualitative analysis only, and the results were analysed using the DIFFRAC.EVA software and the PDF-4+2019 database.

Surface chemical analysis of the surfaces of the columns was performed via X-ray photoelectron spectroscopy (XPS) using a PHI 5500 system (Perkin Elmer, Waltham, Massachusetts, USA). The pressure in the analysis chamber was about 10^{-9} mbar, and the analysed area was about 0.8 mm in diameter. The photoelectrons were generated by a

monochromatic Al Kα source. Energy calibration using Au $4f_{7/2}$ (84.0 eV), Ag $3d_{5/2}$ (368.3 eV), and Cu $2p_{3/2}$ (932.7 eV) was conducted prior to the measurements. High resolution scans were recorded to cover the Ti2p, Al2p, V2p, O1s, N1s, and C1s photoelectron peaks, with a 23.5 eV pass energy with a step of 0.1 eV and nominal take-off angle of 45°. The software PHI Multipak was used for fitting the peaks. Depth profiling was performed by alternating ion etching and XPS analysis. This was performed using argon gas with a 4 kV accelerating voltage, and a 2.5 × 2.5 mm^2 area was rastered. This was calibrated on a flat oxidized tantalum foil.

Finally, to investigate the influence of residual oxygen monitoring on the mechanical properties, 15 tensile samples were built (of 11 mm diameter, see Fig. 1) with and without external control of the L-PBF atmosphere. These were subsequently heat-treated for stress relief in vacuum at 800 °C for 2 h, machined according to DIN 50125 (with a gauge length of 30 mm and gauge diameter of 10 mm) [19], and tested following DIN EN ISO 6892-1 [20] in a certified laboratory (GWP, Dillingen, Saarland, Germany). The build job design allowed for obtaining mechanical properties in dependence on the height, and hence, samples representing five distances from the baseplate were studied. The results are presented with respect to the "Bottom" position corresponding to the lowest sample whose centre is positioned at 8 mm from the baseplate, the "Middle" position corresponding to the 3rd sample at a height of 35 mm and the "Top" position corresponding to the uppermost sample, centre of which is located at a height of 63 mm.

3. Results

3.1. Process atmospheres

The external oxygen monitoring system allows for operating the machine under a very stable oxygen concentration of 100 ppm O_2 measured and monitored using an electrochemical sensor. Fig. 2 displays the variation of the residual oxygen in the process atmosphere when the L-PBF machine regulates the impurity level, recorded by a lambda probe and an electrochemical cell. Both curves display a sinusoidal variation. This sinusoidal type of curve is likely the result of the oxygen closed looped control system of the L-PBF machine, which adjusts the inert gas flow input with the lambda sensor input. The period of the sinusoidal, which informs about the loop delay, increases with time.

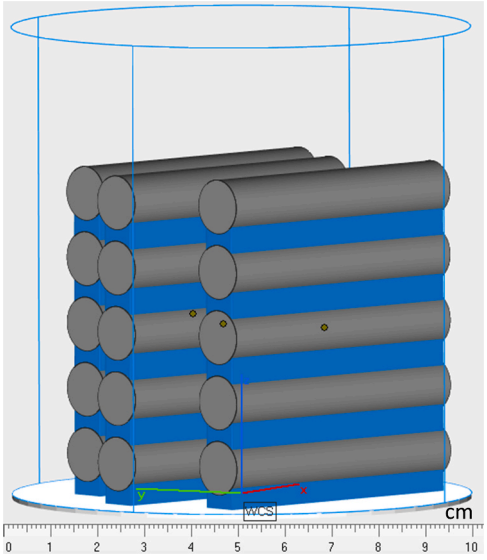

Fig. 1. Design of the build job performed to produce the tensile specimens. The stacking allowed to investigate five distances from the baseplate. From bottom to top, the samples have their centre at heights of 8, 22, 35, 49, and 63 mm. The support structures are presented in blue.

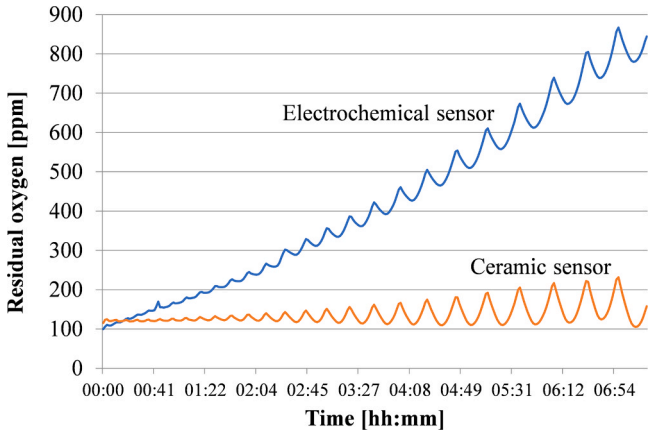

Fig. 2. Oxygen level variations during the L-PBF fabrication of the columns under L-PBF machine-controlled oxygen level.

The control system eventually appears to be unstable during the performed experiment as the signal amplitude increases. The observed oscillation is commonly referred to as a hunting instability, as the oxygen content oscillates around the desired setpoint [21]. The loop delay may also worsen by the longer response time of the lambda sensor after long periods of use [22].

At the beginning of the build job, the values recorded by the lambda sensor oscillate around 120 ppm O_2, and at the end, these are closer to 170 ppm O_2. The starting point being above the targeted value of 100 ppm might be related to the calibration of the sensor or be a result of the control system allowing the process to start, since the oxygen level is quite close to the target value. The hunting instability is recorded by the electrochemical sensor, as well; however, it records a much more important oxygen increase of about 700 ppm compared with 50 ppm recorded by the lambda probe. It is known that the electrochemical oxygen sensor does not exhibit cross-sensitivity for gas species such as H_2 [23]. These differences are further addressed in the discussion section, but it should be kept in mind that the electrochemical sensor depicts more accurately the actual oxygen variations during the build jobs.

3.2. Bulk properties

The virgin powder used to produce both columns contains approximately 1051 ppm O_2 and 150 ppm N_2. Fig. 3(a) and (b) displays the variation in oxygen and nitrogen contents along the height of the columns and in their bulk, produced with the oxygen level controlled by the L-PBF machine and the external monitoring system. It is evident that the oxygen and nitrogen contents follow the same trend regardless of the oxygen monitoring technique. For all, the oxygen and nitrogen concentrations increase with the built height. Oxygen and nitrogen are typically impurities whose concentration varies in a similar manner in the process atmosphere, since it is established by purging the process volume, performing a dilution of these elements. Generally, the ratio of nitrogen to oxygen in the air (of about 4:1) is conserved during the purge. Therefore, one can expect the residual nitrogen to be in the range of 400–3200 ppm. Still, the solubility of oxygen in α-Ti is greater than that of nitrogen, which is consistent with the higher oxygen content reported in the powder and the as-built parts. For the machine-controlled condition, the increase of oxygen and nitrogen in the as-built Ti-6Al-4V with the build height must be connected to the recorded increase of oxygen during the build job, as highlighted by the electrochemical sensor curve in Fig. 2. However, the material produced under the externally controlled oxygen level also exhibits an increase in oxygen and nitrogen content, though to a smaller extent. This suggests that the interstitials pick-up is not caused only by the purity of the process atmosphere in the levels studied. Moreover, it appears to be

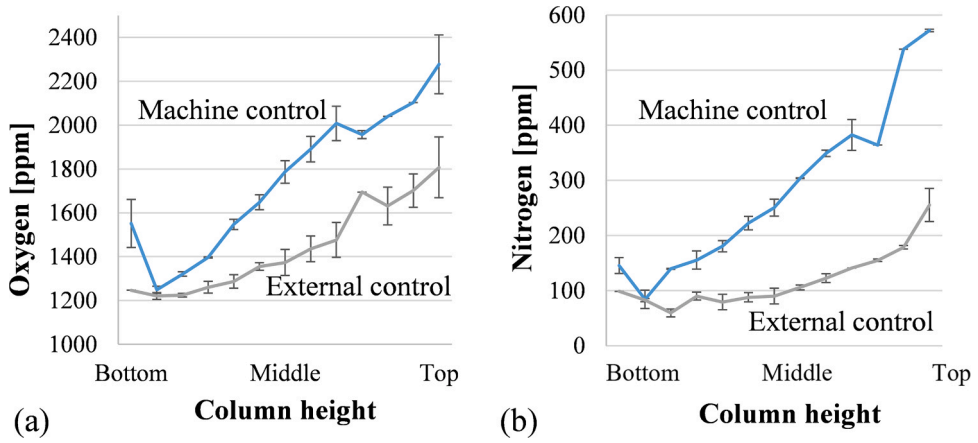

Fig. 3. (a) Oxygen and (b) nitrogen content along the build height of the bulk of the columns built under machine control conditions and when externally control to the oxygen level to 100 ppm O_2. The samples for chemistry were extracted from the centre of the columns.

connected to the high aspect ratio of the produced columns. The heat input is mostly transmitted through the already-solidified material towards the baseplate, which is similar to a heat sink. The powder bed rather acts as an insulating medium. As more layers are deposited, higher heat accumulation takes place. Increased temperature of the material improves the solubility of trace elements due to the enhanced diffusion at increased temperatures and the higher driving force for diffusion. Indeed, 100 ppm of oxygen is orders of magnitude higher than the oxygen potential required to avoid the oxidation of Ti alloys [11]. The presence of higher oxygen contents measured in the produced columns compared with the used powder again confirms that even 100 ppm of oxygen is far above the required oxygen level for Ti-alloys processing by L-PBF to fully avoid pick-up of trace elements. In the case of alloys with lower oxygen affinity, such as 316 L stainless steel, the nitrogen is typically fully transferred while the oxygen is lost [9]. Here, some nitrogen appears to be lost from the powder to the bulk for intermediate build height. For the column produced under stable residual oxygen, it reaches comparable nitrogen levels only towards its top (see Fig. 3). In addition, for both build jobs, an increase of porosity of at least 0.1% (from about 99.9—99.8%) was measured from the bottom to the top of the columns.

Fig. 4 displays the hardness HV10 of the bulk of the Ti-6Al-4V columns along their height. Both columns exhibit an increase of hardness towards the last deposited layers, which may be connected to the increase of oxygen and nitrogen seen in Fig. 3. As could be expected, this hardness increase is not as pronounced when the atmosphere is externally controlled.

Fig. 5 displays the microstructures observed in the bulk of the column produced with 100 ppm residual oxygen. The corresponding microstructures for the second column are not displayed, since they exhibit similar features. The corresponding XRD spectra are displayed in Fig. 6. It appears that the microstructure observed at the top of the columns is characterized by the presence of β phase precipitates appearing with bright contrast between the α/α′lamellas (see Fig. 5(b)). In comparison, the microstructure at the bottom of the columns and up to heights of approximately 50 mm, offers less contrast (Fig. 5(a)), and the pattern of the α/α′fine lamellas can be slightly distinguished. This is the typically obtained as-built microstructure caused by the high cooling rates, while the observed precipitation of the β phase at the top of the column is generally obtained through the partial annealing in the α+β phase field, such as when performing stress-relieving heat treatment (e.g. at 600 °C for 2 h) [17]. These microstructural observations can be connected to the α diffraction peak splitting observed in Fig. 6(b) and more clearly in Fig. 6(c) and (d). This peak splitting has already been demonstrated to be typical of a dual α+α′microstructure obtained by post-heat treatment [24–26]. It was explained that it is induced by the partial decomposition of the martensite through diffusion processes of Al and V. In addition, it is interesting to note that even though such important microstructural differences have not been reported before for a single component built by L-PBF, the effect of build height is already known to be a determinant for various AM processes. It has been demonstrated that the microstructure typically exhibits coarser α lamellas towards the top of tall parts, for both the L-PBF [27] and EBM [28]. Unlike thin geometries, parts with thick cross-sections exhibit finer microstructures, which is attributed to a better heat conductivity towards the heat sink [29]. This in situ decomposition of martensite with height is also accompanied by the detection of the β phase by XRD, as presented in Fig. 6(b). Furthermore, it is known that the dispersion of fine β precipitates induces strengthening, which can also partially explain the hardness increase reported in Fig. 4.

Fig. 7 displays the tensile and yield strength, and the elongation of the Ti-6Al-4V samples built at different distances from the baseplate. While the strength of the samples built under stable residual oxygen content is similar regardless of position (with $Rp_{0.2}$ about 1050 MPa and Rm about 985 MPa), the samples built under machine-controlled atmosphere are stronger when built higher. The yield strength increases by 40 MPa and the tensile strength by 54 MPa when comparing the bottom and top samples. Furthermore, it can be noted that the samples built under steady residual oxygen in the atmosphere are generally weaker but more ductile (with exception at the top position, which may be related to the higher porosity in that set of samples). Also connected to the increase in build height, a reduction of the elongation is observed for both conditions.

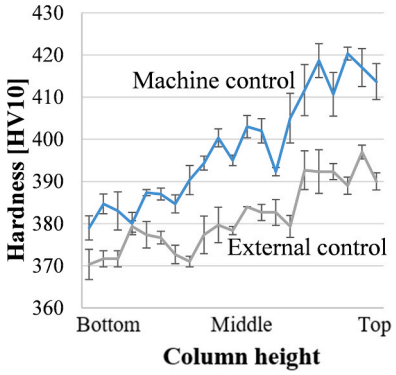

Fig. 4. Evolution of the hardness HV10 of the columns along their built height in the as-built state.

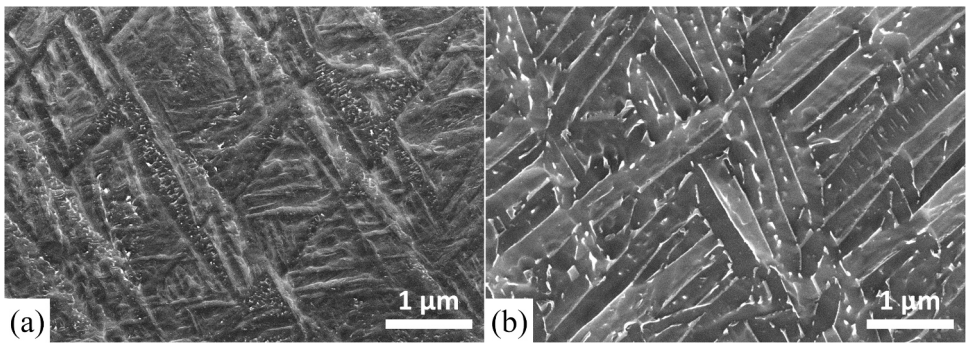

Fig. 5. SEM micrographs, collected with the in-lens secondary electron detector, of the bulk of the column produced under externally controlled residual oxygen for: (a) the bottom position (5 mm from baseplate); and (b) the top position of the column (65 mm from baseplate).

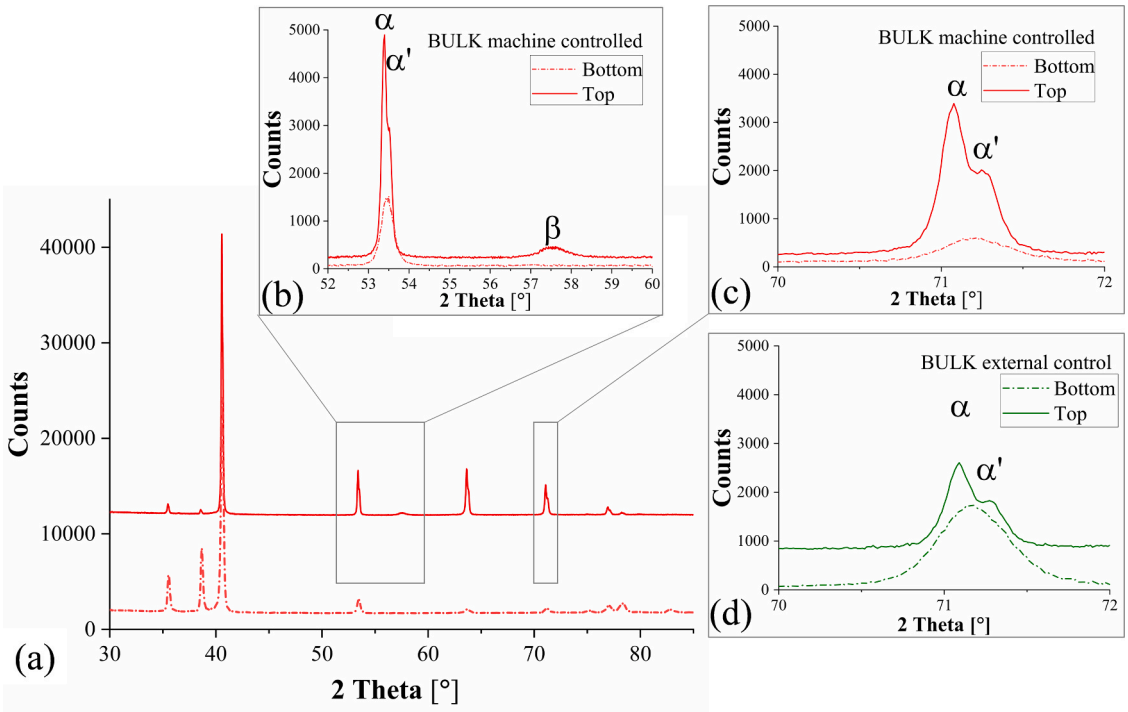

Fig. 6. XRD spectra measured on the polished cross-sections: (a) in the full inspected range for the column produced under machine-controlled oxygen level, at its top and bottom, (b) close-up in the 52–60° range, (c) close-up in the 70–72° range, (d) close- up in the 70–72° range for the column produced with 100 ppm residual oxygen.

3.3. Surface composition

Fig. 8(a) and (c) displays the columns in as-built condition on their baseplate. It is apparent that the increase of atmosphere impurities is reflected in a significant discoloration of the column surface (see Fig. 8c). The effect of the geometry (and heat accumulation) is not so critical, as demonstrated by the uniform colour along the column in Fig. 8(a). Fig. 8(b) and (d) presents the microstructures at the top and close to the column's surface for both atmospheric conditions. It is evident that a 1–2 µm thick scale is observed on the discoloured column. While it is absent under externally controlled residual oxygen (see Fig. 8 (b)), it is thickest at the top of the machine-controlled column and thins towards the baseplate.

The survey spectra of the XPS analysis of the columns' surface indicate the presence of carbon (C1s), nitrogen (N1s), strong titanium (Ti2p), and oxygen (O1s) peaks (see Fig. 9). It shows distinctly higher intensity of the O1s peak for the column produced under standard conditions. For clarity, Fig. 10 displays only the oxygen and nitrogen concentrations for the different surfaces studied. The figure depicts higher oxygen levels on the standard column produced without external oxygen control until the depth of up to 50 nm. Other differences exist between the top and bottom positions of the standard column compared with those of the externally controlled column. The externally controlled column exhibits a lower nitrogen content at the bottom position (close to the baseplate) than at the top position. For both positions, the nitrogen content decreases after 10 nm in a similar manner. For the machine-controlled column, the curve of the nitrogen content for the bottom position suggests a higher starting nitrogen content than for the externally controlled column. Still, after 10 nm, the two columns exhibit similar profiles for nitrogen at the bottom position, while the top position of the machine-controlled column exhibits a notably different profile. While the nitrogen content is low for the first nanometres due to the thicker oxide layer present, it progressively increases to a maximum of about 25 at% around 20 nm. It then slowly decreases deeper but remains above 10 at% at 200 nm.

X-ray diffraction was also conducted on these surfaces (see Fig. 11), even though their curvature makes it difficult to conduct accurate quantitative phase analysis and crystallite size determination [30].

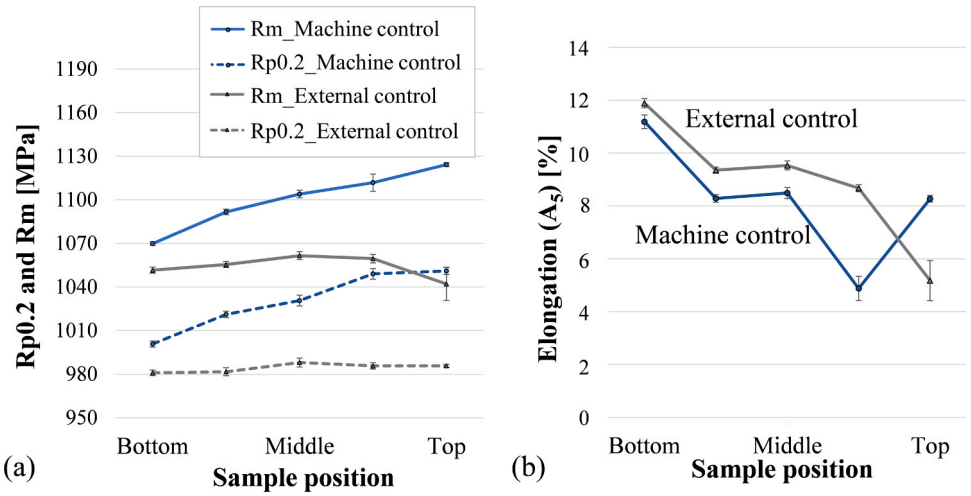

Fig. 7. (a) Tensile strength (R_m), yield strength ($R_{p0.2}$) and (b) elongation (A_5) of the tensile samples positioned at different positions in the build volume.

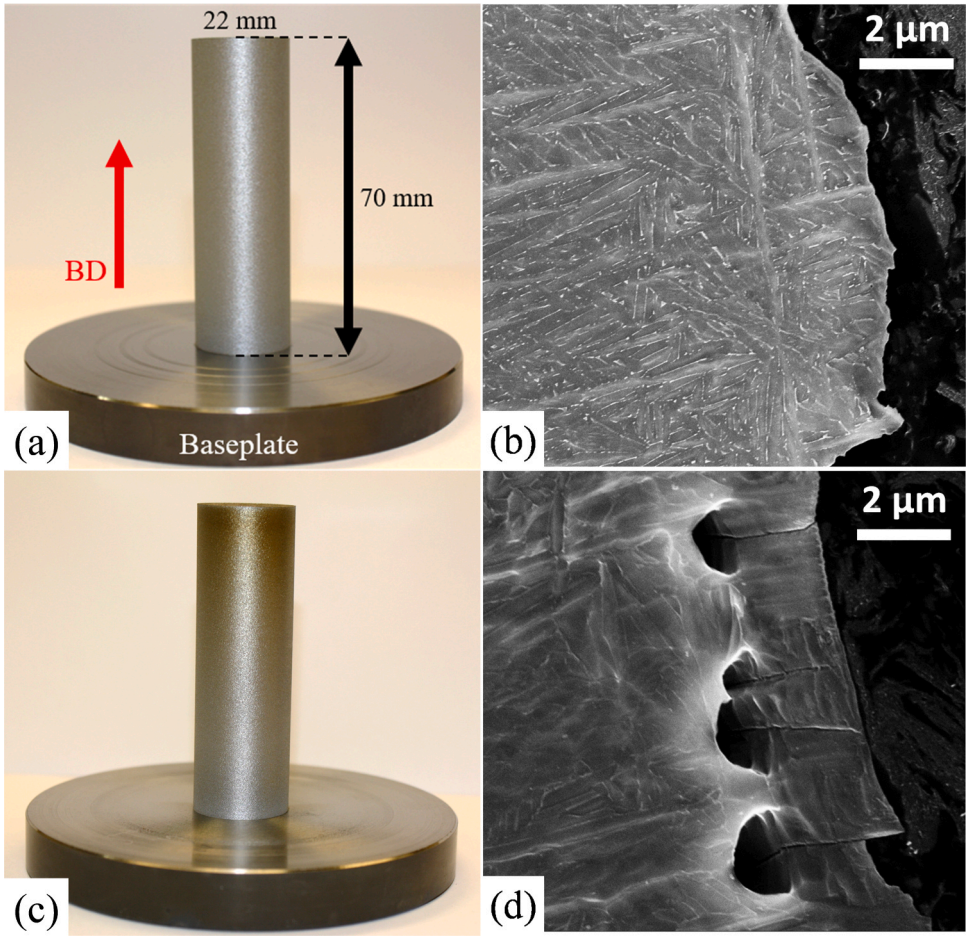

Fig. 8. (a) Photograph of the column built under externally controlled 100 ppm O_2. (b) SEM micrograph of the cross-section at the top of the column built under externally controlled 100 ppm O_2. (c) Photograph of the column built under standard conditions, without external control of the purity of the atmosphere. (d) SEM micrograph of the cross-section at the top of the column built under standard conditions.

Therefore, only peak detection is considered after the background subtraction. As measured on the bulk of the columns (Fig. 6(b)), the β phase is detected for the top surfaces and is connected to the in situ martensite decomposition. The $(103)_\alpha$ peak exhibits a shoulder to its right that is also attributed to the β phase. The other notable differences are three subpeaks for the top machine-controlled surface close to 43°, 47.5°, and 48.5°.

4. Discussions

The oxygen variation recordings suggest higher reliability of an electrochemical sensor compared with the lambda oxygen sensor that

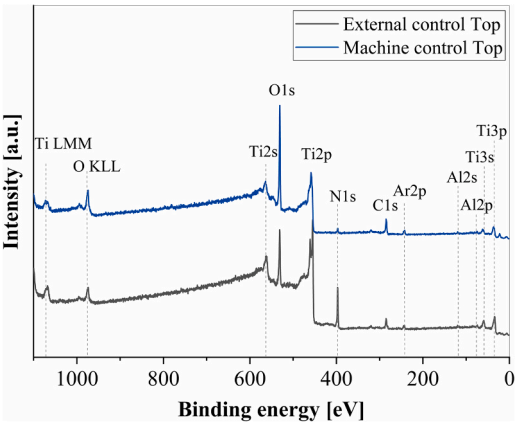

Fig. 9. XPS survey spectra of the top positions of the two investigated columns after surface contamination removal with Ar^+ etching.

would allow for improving the oxygen control system of the L-PBF machine (see Fig. 2). The ceramic sensors are widely employed within the industrial oxygen control systems and exhaust emission control systems of cars [23]; still, their performance is known to degrade in the presence of H_2, CO, NO, and hydrocarbons [31]. They are typically comprised of a doped solid ceramic electrolyte (such as yttrium stabilized zirconia) and two platinum electrodes on opposite sides of the ceramic exposed to the process gas (exhaust gases for a car) and the reference atmosphere (where P_{O2} = 0.21 bar) [22]. Both sides are gas-tight from each other, and the side exposed to the process is protected by a porous ceramic layer. Different oxygen chemical potentials develop at each electrode according to the Nernst's equation. Thus, by maintaining a constant reference oxygen partial pressure, the signal of a balanced lambda sensor depends only on its temperature. The typical operating temperature is high –approximately 700 °C [22]. The inconsistency of the lambda probe output with the presence of hydrogen and hydrocarbon is connected to their oxidation on the hot sensor head [31]. This results in lower oxygen concentration at the platinum electrode and therefore the sensor underestimates the actual oxygen present during the process. Unlike the lambda probe, electrochemical cells do not exhibit such cross-sensitivity. While the sinusoidal variations can be attributed to the oxygen control system, the increase in oxygen over the build job cannot be. It has been demonstrated that when the lambda probe records a 50 ppm O_2 increase, the electrochemical cell measures a 700 ppm O_2 increase. This underestimation of the lambda probe can be attributed to the presence of hydrogen. Hydrogen is likely to come from water vapour present in the process atmosphere. Water vapour itself may come from the starting humidity in the atmosphere and the adsorbed humidity on the powder and machine interior. The Ti-6Al-4V powder particles themselves might be a source of hydrogen because of moisture adsorption [32]. Finally, leakages of the machine, such as through its door or in its gas recirculation system might be a source of water vapour, as well. The electrochemical cell measurements highlight that the oxygen level increases significantly at a relatively constant rate of approximately 1.7 ppm O_2/min for 7 h. By employing an optimized

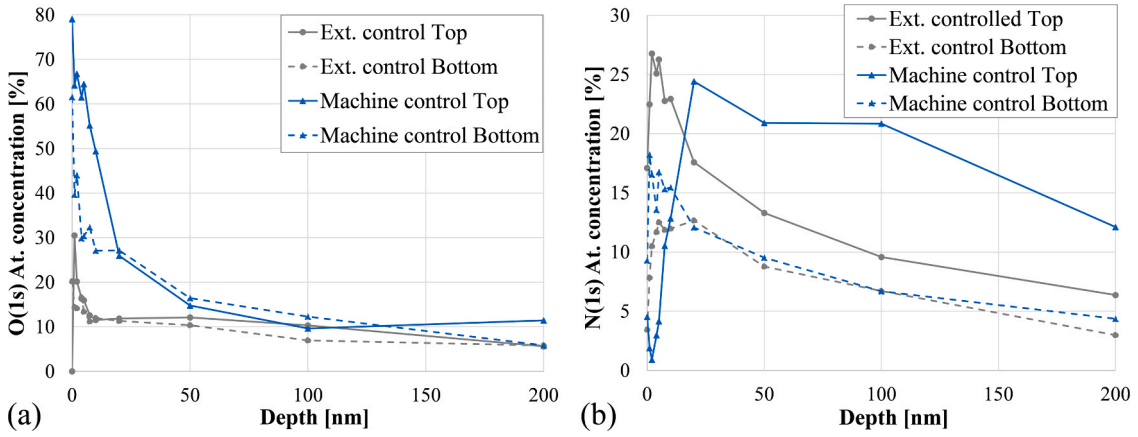

Fig. 10. Profile of (a) O(1s) and (b) N(1s) atomic concentration for the top and bottom positions of the two investigated columns.

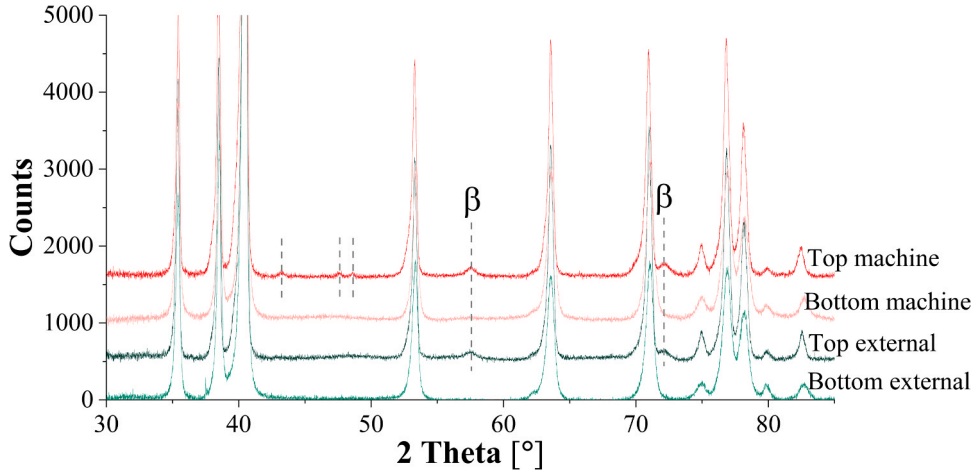

Fig. 11. XRD analysis on the surfaces of the Ti-6Al-4V columns produced under external controlled and machine-controlled oxygen level.

oxygen control system and an electrochemical sensor, such an increase in residual oxygen can be avoided. It was revealed that the produced material under standard conditions is characterized by a gradient in oxygen and nitrogen along its building direction, which is more critical than under a controlled residual oxygen of 100 ppm. From Fig. 3(a) and (b), it can be inferred that this increase is about 16 ppm O_2/mm and 7 ppm N_2/mm along the column height, while it is only about 9 ppm O_2/mm and 2 ppm N_2/mm for the column produced under the controlled atmosphere. It should be underlined that number of commercially available L-PBF systems are already using a combination of for example two electrochemical samples, whose output data are recorded and monitored during the process. Improvements connected to the precision calibration of these sensors at relevant oxygen levels could still be implemented.

The external oxygen control system also recorded the variation in dew point during the printing processes. These are relatively minor and demonstrate an increase from −31 °C to −24 °C during the 7 h build job under standard processing conditions or an H_2O content from 280 ppm to 540 ppm. This increase is slightly smaller when the oxygen is externally monitored: from −32 °C to −28 °C or an H_2O content from 260 ppm to 370 ppm. In addition, the variations in hydrogen content in the bulk of the as-built columns along the build height are minimal. This level remains at approximately 40 ppm H_2, which is still higher than the 17 ppm present in the virgin powder but lower than the limit of 150 ppm defined in the ASTM F2924-14 [33]. Hydrogen is a strong β stabilizing element, and its solubility can reach as high as 50 at% above 600 °C, while it is only 7 at% in α at 300 °C and decreases rapidly with lower temperatures [34]. The limited solubility and diffusion of hydrogen in the α phase combined with the rapid cooling from the β phase during the L-PBF process are likely to explain the similar and relatively low H_2 contents measured in both columns.

The presented results confirm that heat accumulation occurs as the material is solidified further from the baseplate, leading to lower cooling rates and high temperature retention during the solid-state cooling process. Both the XRD of the bulk and surfaces and the microstructural analysis indicate in situ partial decomposition of the martensite. In addition, the increase in oxygen by around 600 ppm and nitrogen by around 180 ppm along the built height of the column produced under constant 100 ppm residual oxygen suggests that the high temperature retention facilitated the higher interstitial dissolution from a kinetic point of view. Indeed, thermodynamically, the oxygen potential is high enough to promote interstitials pick-up. Fig. 12 displays the thermodynamic simulation of the oxygen and nitrogen solubility in Ti-6Al-4V. It indicates that both oxygen and nitrogen impurities have a high solubility in the matrix, about 17 at% and 12 at% at 1000 °C, respectively.

Both the decomposition of the martensite and the pick-up of interstitials contribute to the hardness increase (additional 20 HV10) along the build height of the externally controlled column (see Fig. 4). As reported by de Formanoir et al. [26] and Pauzon et al. [17], the formation of fine β precipitates induces substantial strengthening. Since a similar contribution of β precipitation on the hardness for both columns is expected, the hardness difference between both (25 HV10 at the top) can be understood only by considering their differences in oxygen (500 ppm at the top) and nitrogen (330 ppm at the top) contents, which are connected only to the atmosphere composition, indicated during monitoring. Even though oxygen and nitrogen are known to be strong α phase stabilizers, the effect of heat accumulation appears to be the dominant driver for the martensite decomposition in this case. In addition, the calculation of the lattice parameter of the α phase from the XRD data collected on the bulk of the columns highlights that the oxygen and nitrogen absorption did not result in lattice expansion as expected [35] (see Table 2). Furthermore, the α peak splitting observed is very similar for both columns: with a 0.148° split for the machine-controlled column and a 0.143° split for the externally controlled column on the $(103)_\alpha$ peak. Still, it is evident that the pick-up of oxygen and nitrogen, owing to the poor control of the atmosphere, contributes to the increased hardness (see Fig. 4), likely due to hardening of the α phase,

Table 2
Evaluation of the XRD spectra of the bulk of the Ti-6Al-4V columns: Lattice parameter a is calculated from peak $(100)_\alpha$, and lattice parameter c is calculated from peak $(002)_\alpha$.

	a [Å]	c [Å]	c/a
Top ext. control	2.9171	4.6621	1.5982
Bottom ext. control	2.9188	4.6584	1.5960
Top machine control	2.9179	4.6604	1.5972
Bottom machine control	2.9134	4.6533	1.5972

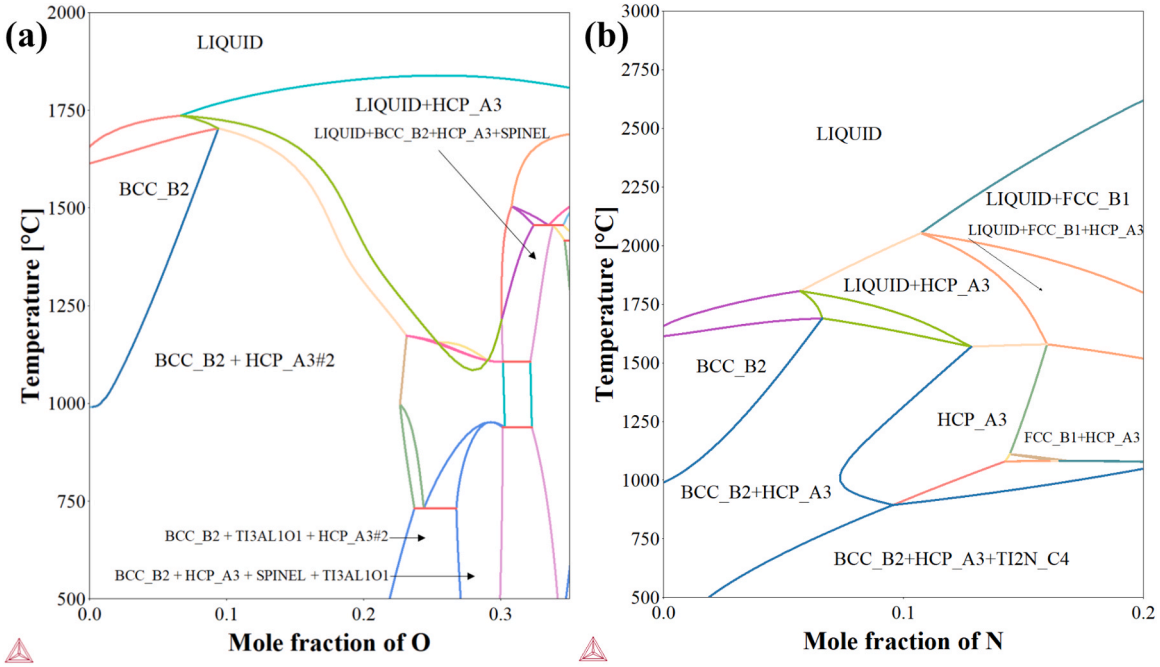

Fig. 12. (a) Ti-6Al-4V and O and (b) Ti-6Al-4V and N phase diagrams plotted with Thermo-Calc 2020b using the TCTI2 and TCOX10 database for Ti alloys (v2.2).

since oxygen and nitrogen occupy the octahedron and tetrahedron interstitial sites [13,14]. This is likely to be detrimental to the already-limited ductility of Ti-6Al-4V built by L-PBF and can promote embrittlement of the produced component, which is undesirable for medical applications, such as reported for thin samples by Barba et al. [15]. This hazard has also been put in evidence by Velasco-Castro et al. [16], who produced Ti-6Al-4V lattice structures enriched in oxygen using a tailored scanning strategy, resulting in reduced ductility and thus reduced compressive strength. This is also confirmed in the presented work (see Fig. 7), as strength increases significantly with the increase of impurities in the atmosphere and hence in the material, which is accompanied by a reduced elongation at break. The observed reduction in density towards the top of the columns is suspected to be connected to the increased oxygen content and hence a possible increased melt pool instability.

The discoloration of the column produced using machine control is associated with the additional oxygen and nitrogen pick-up due to the atmosphere's impurities and the formation of an oxygen- and nitrogen-rich outer layer surface, as analysed by XPS and observed by SEM (see Figs. 10 and 8(d)). It should be kept in mind that the investigated depth by XPS is smaller than the layer observed on the micrograph. In addition, this discoloration is not accounted in the measured mechanical properties which were evaluated on the machined tensile specimens. Several post-processing techniques could be envisaged to remove or modify this oxygen- and nitrogen-rich layer such as, sandblasting, shot peening, or even manual grinding or machining. However, this would not counteract the oxygen and nitrogen dissolution in the bulk, which is more detrimental regarding the mechanical properties. It should be kept in mind that discolorations on the surface of Ti-6Al-4V are often used as exclusion criteria after welding (for example [36,37]). It appears that particles are present at the interface between the scale and the matrix in the case of the discoloured component and that channels connect these particles and the surface of the component through the scale. Even though the curvature of the surfaces limits accurate peak identification on the spectra presented in Fig. 11, by applying a chemical filter on the PDF database, several candidates are proposed. With several diffraction peaks in the 42–50° range, TiN (PDF 00-002-1221) and Al_2O_3 (PDF 00-003-0914) appear to be the most reliable candidates. Transmission electron microscopy could support the proper identification of these particles. Even though it is beyond the scope of the present study, it would be interesting to study the effect of oxygen and nitrogen present in the process atmosphere on the other properties. Nitriding of Ti-6Al-4V has been widely investigated as an effective means of improving tribological properties [38] and limiting the inward diffusion of oxygen [39]. For example, Valente et al. [40] recently studied the effect of nitriding and carbo-oxidising on the wear resistance of Ti-6Al-4V produced by L-PBF. This study revealed that these treatments are promising in reducing the specific wear volume tested by dry sliding friction against Al_2O_3. Finally, it should be kept in mind that the observed discoloration could be mitigated by an adjustment of the heat input through the laser parameters adjustment. Of course, this may imply further changes in the properties of the AM-produced material.

5. Conclusions

The present study confirms that a robust oxygen control system is necessary under the L-PBF conditions investigated, to establish and maintain a stable high purity process atmosphere and limit an additional pick-up of impurities, especially when processing alloys sensitive to oxidation, such as Ti-6Al-4V. The following conclusions can be drawn:

- It was proven that an increase in oxygen and nitrogen levels in the processing atmosphere results in a direct increase in oxygen and nitrogen in the as-built material. As an oxygen increase at a rate of about 1.7 ppm/min in the atmosphere was registered, increases of about 16 ppm O_2/mm and 7 ppm N_2/mm along the column height are reported.
- This increased pick-up under standard conditions without the use of an external monitoring system contributed to the hardening to an extent of about 25 HV10 at a full height of 70 mm. When the oxygen is maintained at 100 ppm in the atmosphere, the uptake is decreased by almost half to 9 ppm O_2/mm and 2 ppm N_2/mm along the column height.
- The decreasing quality of the process atmosphere on the laboratory scale L-PBF machine was also connected to a discoloration of the surface of the column. This was attributed to the development of a few-μm-thick layer rich in oxygen and especially nitrogen, as was proven by the XPS analysis and SEM cross-section study of the specimen.
- It was revealed that the column geometry promoted heat accumulation with increasing height of the specimen. This was also confirmed by the partial decomposition of martensite, observed by the microstructural and XRD investigations. This heat accumulation can be held partially responsible for the enhanced oxygen and nitrogen pick-up. This contribution is estimated to approximately a 600 ppm O_2 and 150 ppm N_2 difference between the bottom and top of the sample of 70 mm height.
- Both the fine precipitation of the β phase and the pick-up of interstitials led to an increase of hardness of about 20 HV10 at full height. This was also reflected in the mechanical response of the produced Ti-6Al-4V material, which experienced significant embrittlement when produced without oxygen control on the studied machine–an increase of about 50 MPa in strength and a reduction of 4% in elongation after stress relief.

CRediT authorship contribution statement

Camille Pauzon: Methodology, Validation, Formal analysis, Investigation, Data curation, Writing - original draft and review & editing. **Kai Dietrich:** Methodology, Conceptualization, Formal analysis, Investigation, Data curation, Writing - review & editing. **Pierre Forêt:** Resources, Supervision, Project administration. **Sophie Dubiez-Le Goff:** Validation, Formal analysis. **Eduard Hryha**: Formal analysis, Methodology, Supervision, Writing - review & editing, Project administration. **Gerd Witt:** Supervision, Project administration.

Declaration of Competing Interest

The authors declare that they have no known competing financial interests or personal relationships that could have appeared to influence the work reported in this paper.

Acknowledgments

This work has been conducted in the framework of the Centre for Additive Manufacturing – Metal (CAM^2) supported by the Swedish Governmental Agency of Innovation Systems (Vinnova). Additional support from Production Area of Advance at Chalmers University of Technology has been received. In addition, the authors are grateful to Andreas Markström for his support with the Thermo-Calc calculations.

References

[1] P. Bidare, I. Bitharas, R.M. Ward, M.M. Attallah, A.J. Moore, Laser powder bed fusion in high-pressure atmospheres, Int. J. Adv. Manuf. Technol. 99 (2018) 543–555, https://doi.org/10.1007/s00170-018-2495-7.
[2] C. Zhao, K. Fezzaa, R.W. Cunningham, H. Wen, F. De Carlo, L. Chen, A.D. Rollett, T. Sun, Real-time monitoring of laser powder bed fusion process using high-speed X-ray imaging and diffraction, Sci. Rep. 7 (2017) 3602, https://doi.org/10.1038/s41598-017-03761-2.
[3] Q. Guo, C. Zhao, L.I. Escano, Z. Young, L. Xiong, K. Fezzaa, W. Everhart, B. Brown, T. Sun, L. Chen, Transient dynamics of powder spattering in laser powder bed fusion additive manufacturing process revealed by in-situ high-speed high- energy

x-ray imaging, Acta Mater. 151 (2018) 169–180, https://doi.org/10.1016/j.actamat.2018.03.036.
[4] M.P. Haines, N.J. Peter, S.S. Babu, E.A. Jägle, In-situ synthesis of oxides by reactive process atmospheres during L-PBF of stainless steel, Addit. Manuf. 33 (2020), 101178, https://doi.org/10.1016/j.addma.2020.101178.
[5] A. Ladewig, G. Schlick, M. Fisser, V. Schulze, U. Glatzel, Influence of the shielding gas flow on the removal of process by-products in the selective laser melting process, Addit. Manuf. 10 (2016) 1–9, https://doi.org/10.1016/j.addma.2016.01.004.
[6] M. Schniedenharn, J.H. Schleifenbaum, On the Correlation of the Shielding Gas Flow in L-PBF Machines with Part Density, (2018) 1–7.
[7] Renishaw, Our technology, (n.d.). ⟨http://www.renishaw.com/en/our-technology–27362⟩ (accessed March 28, 2018).
[8] K. Dietrich, J. Diller, S.D. Go, D. Bauer, P. Forêt, The Influence of Oxygen on the Chemical Composition and Mechanical Properties of Ti-6Al-4V during Laser Powder Bed Fusion (L-PBF), 32 (2020). doi:10.1016/j.addma.2019.100980.
[9] C. Pauzon, E. Hryha, P. Forêt, L. Nyborg, Effect of argon and nitrogen atmospheres on the properties of stainless steel 316L parts produced by laser-powder bed fusion, Mater. Des. 179 (2019), 107873, https://doi.org/10.1016/j.matdes.2019.107873.
[10] F. Suska, G. Kjeller, P. Tarnow, E. Hryha, L. Nyborg, A. Snis, A. Palmquist, Electron beam melting manufacturing technology for individually manufactured jaw prosthesis: a case report, J. Oral Maxillofac. Surg. 74 (2016) 1706.e1–1706.e15, https://doi.org/10.1016/j.joms.2016.03.046.
[11] E. Hryha, R. Shvab, M. Bram, M. Bitzer, L. Nyborg, Surface chemical state of Ti powders and its alloys: effect of storage conditions and alloy composition, Appl. Surf. Sci. 388 (2016) 294–303, https://doi.org/10.1016/j.apsusc.2016.01.046.
[12] E. Hryha, R. Shvab, M. Bram, M. Bitzer, L. Nyborg, Surface chemical state of Ti powders and its alloys: effect of storage conditions and alloy composition, Appl. Surf. Sci. 388 (2016) 294–303, https://doi.org/10.1016/j.apsusc.2016.01.046.
[13] Q. Yu, L. Qi, T. Tsuru, R. Traylor, D. Rugg, J.W. Morris, M. Asta, D.C. Chrzan, A. M. Minor, Origin of dramatic oxygen solute strengthening effect in titanium, Science 347 (2015) 635–639, https://doi.org/10.1126/science.1260485.
[14] G. Lütjering, J.C. Williams, Titanium: Engineering Materials and Processes, 2nd ed., Springer, 2007, pp. 1–442, https://doi.org/10.1007/978-3-540-73036-1.
[15] D. Barba, C. Alabort, Y.T. Tang, M.J. Viscasillas, R.C. Reed, E. Alabort, On the size and orientation effect in additive manufactured Ti-6Al-4V, Mater. Des. 186 (2020), 108235, https://doi.org/10.1016/j.matdes.2019.108235.
[16] M. Velasco-Castro, E. Hernández-Nava, I.A. Figueroa, I. Todd, R. Goodall, The effect of oxygen pickup during selective laser melting on the microstructure and mechanical properties of Ti–6Al–4V lattices, Heliyon 5 (2019), e02813, https://doi.org/10.1016/j.heliyon.2019.e02813.
[17] C. Pauzon, P. Forêt, E. Hryha, T. Arunprasad, L. Nyborg, Argon-helium mixtures as laser-powder bed fusion atmospheres: towards increased build rate of Ti-6Al-4V, J. Mater. Process. Technol. 279 (2020), 116555, https://doi.org/10.1016/J.JMATPROTEC.2019.116555.
[18] K. Dietrich, P. Forêt, D. Bauer, G. Witt, How Porosity Is Affected By Different Residual Oxygen Concentrations in the Building Chamber During Laser Powder Bed Fusion (L-PBF). EPMA, EuroPM2018,, Bilbao, 2018.
[19] DIN 50125 - Testing of Metallic Materials - Tensile Test Pieces, (n.d.).
[20] DIN EN ISO 6892–1:2016 - Metallic Materials - Tensile Testing - Part 1: Method of test at room temperature, (2017).
[21] The Editors of Encyclopaedia Britannica, Control system, Encycl. Br. (2013). ⟨https://www.britannica.com/technology/control-system⟩.
[22] P. Shuk, Zirkondioxid-sauerstoffsensoren - Stand der technik, Technol. Mess 77 (2010) 19–23, https://doi.org/10.1524/teme.2010.0003.
[23] C.O. Park, S.A. Akbar, W. Weppner, Ceramic electrolytes and electrochemical sensors, J. Mater. Sci. 38 (2003) 4639–4660, https://doi.org/10.1023/A:1027454414224.
[24] S. Cao, R. Chu, X. Zhou, K. Yang, Q. Jia, Role of martensite decomposition in tensile properties of selective laser melted Ti-6Al-4V, J. Alloy. Compd. 744 (2018) 357–363, https://doi.org/10.1016/j.jallcom.2018.02.111.
[25] K. Sofinowski, M. Šmíd, I. Kuběna, S. Vivès, N. Casati, S. Godet, H. Van, Swygenhoven, In situ characterization of a high work hardening Ti-6Al-4V prepared by electron beam melting, Acta Mater. 179 (2019) 224–236, https://doi.org/10.1016/j.actamat.2019.08.037.
[26] C. de Formanoir, G. Martin, F. Prima, S.Y.P. Allain, T. Dessolier, F. Sun, S. Vivès, B. Hary, Y. Bréchet, S. Godet, Micromechanical behavior and thermal stability of a dual-phase α+α' titanium alloy produced by additive manufacturing, Acta Mater. 162 (2019) 149–162, https://doi.org/10.1016/j.actamat.2018.09.050.
[27] E.W. Lui, W. Xu, A. Pateras, M. Qian, M. Brandt, New Development in Selective Laser Melting of Ti – 6Al – 4V: A Wider Processing Window for the Achievement of Fully Lamellar a + b Microstructures, 69 (2017) 2679–2683. doi:10.1007/s11837–017-2599–9.
[28] P. Wang, M. Ling, S. Nai, W.J. Sin, J. Wei, Effect of Building Height on Microstructure and Mechanical Properties of Big-Sized Ti-6Al-4V Plate Fabricated by Electron Beam Melting, 1 (2015) 4–7.
[29] T. Machry, D. Eatock, J. Meyer, A. Antonysamy, A. Ho, P. Prangnell, D. Eatock, J. Meyer, A. Antonysamy, A. Ho, P. Prangnell, T. Machry, D. Eatock, J. Meyer, A. Antonysamy, A. Ho, P. Prangnell, Effect of Microstructure on the Tensile Strength of Ti6al4v Specimens Manufactured Using Additive Manufacturing Electron Beam Process Effect of Microstructure on the Tensile Strength of Ti6al4v Specimens Manufactured Using Additive Manufacturing Electron, 5899 (2016). doi:10.1080/00325899.2015.1123800.
[30] A.O. Zhigachev, The effect of specimen surface curvature on x-ray diffraction peak profiles, Rev. Sci. Instrum. 84 (2013), 095105, https://doi.org/10.1063/1.4820444.
[31] E. Hryha, L. Nyborg, Process control system for delubrification of PM steels, Acta Metall. Slov. 18 (2012) 60–68.
[32] A. Hodgson, S. Haq, Water adsorption and the wetting of metal surfaces, Surf. Sci. Rep. 64 (2009) 381–451, https://doi.org/10.1016/j.surfrep.2009.07.001.
[33] ASTM-International, ASTM F2924–14: Standard Specification for Additive Manufacturing Titanium-6 Aluminum-4 Vanadium with Powder Bed Fusion, (2017) 1–9. doi:10.1520/F2924–14.2.
[34] E. Tal-Gutelmacher, D. Eliezer, The hydrogen embrittlement of titanium-based alloys, JOM 57 (2005) 46–49, https://doi.org/10.1007/s11837-005-0115-0.
[35] R. Montanari, G. Costanza, M.E. Tata, C. Testani, Lattice expansion of Ti-6Al-4V by nitrogen and oxygen absorption, Mater. Charact. 59 (2008) 334–337, https://doi.org/10.1016/j.matchar.2006.12.014.
[36] DIN 29591 Beiblatt 1, Prüfung von Schweißern, 1996.
[37] J.P. Bergmann, Laserstrahlschweißen von titanwerkstoffen unter berücksichtigung des einflusses des sauerstoffes, Materwiss. Werksttech. 35 (2004) 543–556, https://doi.org/10.1002/mawe.200400776.
[38] S.R. Hosseini, A. Ahmadi, Evaluation of the effects of plasma nitriding temperature and time on the characterisation of Ti_6Al_4V alloy, Vacuum 87 (2013) 30–39, https://doi.org/10.1016/j.vacuum.2012.06.008.
[39] P. Pérez, Influence of nitriding on the oxidation behaviour of titanium alloys at 700 °C, Surf. Coat. Technol. 191 (2005) 293–302, https://doi.org/10.1016/j.surfcoat.2004.04.066.
[40] E.H. Valente, M.S. Jellesen, M.A.J. Somers, T.L. Christiansen, Gaseous surface hardening of Ti-6Al-4V fabricated by selective laser melting, Surf. Coat. Technol. 383 (2020), 125278, https://doi.org/10.1016/j.surfcoat.2019.125278.